Ground Testing for Hypervelocity Flow, Capabilities and Limitations

Hans G. Hornung
Graduate Aerospace Laboratories
California Institute of Technology

March 29, 2010

Contents

Report Documentation Page

Form Approved
OMB No. 0704-0188

1. REPORT DATE	2. REPORT TYPE	3. DATES COVERED
APR 2010	**N/A**	**-**

4. TITLE AND SUBTITLE	5a. CONTRACT NUMBER
Ground Testing for Hypervelocity Flow, Capabilities and Limitations	5b. GRANT NUMBER
	5c. PROGRAM ELEMENT NUMBER
6. AUTHOR(S)	5d. PROJECT NUMBER
	5e. TASK NUMBER
	5f. WORK UNIT NUMBER
7. PERFORMING ORGANIZATION NAME(S) AND ADDRESS(ES) **Graduate Aerospace Laboratories California Institute of Technology**	8. PERFORMING ORGANIZATION REPORT NUMBER
9. SPONSORING/MONITORING AGENCY NAME(S) AND ADDRESS(ES)	10. SPONSOR/MONITOR'S ACRONYM(S)
	11. SPONSOR/MONITOR'S REPORT NUMBER(S)

12. DISTRIBUTION/AVAILABILITY STATEMENT
Approved for public release, distribution unlimited

13. SUPPLEMENTARY NOTES
See also ADA569031. Aerothermodynamic Design, Review on Ground Testing and CFD (Conception aerothermodynamique, revue sur les essais au sol et dynamique des fluides informatisee).

14. ABSTRACT

15. SUBJECT TERMS

16. SECURITY CLASSIFICATION OF:			17. LIMITATION OF ABSTRACT	18. NUMBER OF PAGES	19a. NAME OF RESPONSIBLE PERSON
a. REPORT	b. ABSTRACT	c. THIS PAGE			
unclassified	**unclassified**	**unclassified**	**SAR**	**26**	

CONTENTS CONTENTS

1 Introduction

In this document the requirements for ground simulation of hypervelocity flows are set out on the basis of the similarity parameters of the problem. This, together with the thermodynamical properties of the gas in question, the consequent heat loads on the facility and large power requirements, leads to the two most successful devices, the reflected shock tunnel and the expansion tube. After a description of the operation and the thermodynamics of these devices, their essential limitations are explained. Scale effects of these limitations are discussed. On this basis the range over which they can be applied for flow simulation is delineated.

The term *high-enthalpy* or *hypervelocity* flow is used to distinguish those flows in which the velocity is so large that the conditions after the bow shock on a body are such as to cause the molecular components of the gas to dissociate. The fields of human endeavor where high-enthalpy flows are of importance are those in which an object traverses the atmosphere of one of the planets of the solar system. Typically this could be associated with transport to or from space in man-made vehicles, but high-enthalpy flows also occur naturally, *e. g.*, when a meteorite enters a planetary atmosphere.

The term *hypersonic* flow is used to describe situations where the flow speed is large compared to the free-stream speed of sound. Such high-Mach-number flows can, of course, be generated by lowering the speed of sound by lowering the temperature. The low temperature limit is the boiling point of the gas. In such *cold* hypersonic flows, the important dissociative and other real-gas effects of hypervelocity flows do not occur. In order to understand the intricacies of flows in which the chemistry of the gas is activated by the kinetic energy of the flow, it is necessary to simulate *high-enthalpy* flows in the laboratory.

In the context of the earth the lowest orbital velocity is about 8 km/s. The heat flux to a body scales like ρU^3, where ρ is the gas density and U the velocity. As a body enters the atmosphere and moves to lower altitudes, U decreases and ρ increases. At a velocity of approximately 6 km/s the heat flux reaches a maximum. In the frame of reference of the flying object, the ordered kinetic energy per unit mass of the free-stream gas at this speed is therefore $U^2/2 = 18$ MJ/kg. At high enthalpy, the Mach number, which measures the square root of the ratio of the ordered kinetic energy of the flow to the thermal energy of the gas, is not so important as the ratio of the ordered kinetic energy measured in terms of the specific dissociation energy of the gas. There are usually several such characteristic chemical energies.

The characteristic specific energies relevant for air are

$$\begin{array}{rclrcl} D_{\mathrm{N_2}} & = & 33.6\ \mathrm{MJ/kg} & E_{\mathrm{vN_2}} & = & 0.992\ \mathrm{MJ/kg} \\ D_{\mathrm{O_2}} & = & 15.5\ \mathrm{MJ/kg} & E_{\mathrm{vO_2}} & = & 0.579\ \mathrm{MJ/kg} \\ D_{\mathrm{NO}} & = & 20.9\ \mathrm{MJ/kg} & E_{\mathrm{vNO}} & = & 0.751\ \mathrm{MJ/kg} \end{array}$$

where the D's and E_{v}'s are specific energies of dissociation and of vibration respectively. It is not possible to simulate the numerous idiosyncrasies of a particular gas by using another gas. The specific chemical energies have definite fixed values, and the duplication of the ratios of the ordered kinetic energy to them in a simulation implies that *the actual flow speed has to be duplicated.*

It follows that the specific reservoir enthalpy h_0 of the flow (sometimes called total enthalpy), which is approximately equal to $U^2/2$, has to have the same value as in flight.

1 INTRODUCTION

If the flow is accelerated from a reservoir at rest through a nozzle expansion, without adding energy to it during the expansion, the specific reservoir enthalpy corresponding to a flow speed of 6 km/s is 18 MJ/kg, which, at a reservoir pressure of 100 MPa, implies a temperature of nearly 9000 K in air.

The high pressure is necessary to ensure that the chemical reaction rates occur at the right speed for correct simulation of nonequilibrium effects. Smaller scale requires faster reaction for correct simulation. If the temperatures are right (as is ensured by correct flow speed) the reaction rates depend mainly on the density. Rates for binary reactions, like dissociation, are linear in density, those for three-body reactions, like recombination, are quadratic in density. Thus, all reactions can never be simulated correctly except at full scale. In many cases, three-body reactions are not important and, where they are, component testing or extrapolation is necessary.

Continuous flow facilities are ruled out by the high power requirements of typically a few GW. The high speed reduces the steady flow duration requirement to a few ms, however. A convenient way to accelerate, heat and compress a gas for a short time, is to propagate a shock wave through it. Many types of high-enthalpy facilities therefore embody shocks as elements for generating high enthalpy and pressure.

The problem of high-enthalpy simulation is not limited to speeds of the order of 6 km/s, of course. Meteorites entering planetary atmospheres typically have a speed of 20 km/s, and proposals for man-made vehicles have considered speeds in the vicinity of 16 km/s. Such conditions involve very strong ionization of the gas and intense radiative heating. In the following discussion, such very high speeds will not be considered, and attention will be concentrated on the range 3-7 km/s. In this range, the requirements for simulation of hypervelocity flows and some of the methods by which the simulation has been achieved to date will be presented. The document then closes with a discussion of the limitations and achieved conditions of the different types of facilities.

This document gives a descriptive account of the reasons for the forms that hypervelocity simulation facilities have taken. It is not a detailed account of the work that has been done in the field, and only a few representative publications will be cited. An important book on the subject is Lukasiewicz (1973). The interested reader should consult this volume on questions concerning this field.

2 Requirements for Ground Simulation

2.1 Similarity

2.1.1 General Considerations

To simulate a high-enthalpy flow over a body using a model at smaller scale, all the dimensionless parameters of the problem have to be reproduced. In steady hypervelocity flows any dimensionless dependent quantity Q, say, depends on dimensionless variables as follows:

$$Q = Q(M_\infty, Re, Pr, T_w/T_0, B_n, \alpha, \beta, E_i, R_j, Le_i, c_{\infty i}).$$

Here, M_∞ is the free stream Mach number, Re and Pr are Reynolds and Prandtl numbers, which, in this context, are best defined at conditions corresponding to the gas in equilibrium after a normal shock for which the upstream conditions are those of the free stream, T_w is a representative body surface temperature, T_0 is the temperature from which a gas would have to be expanded by a steady expansion to reach the free-stream conditions, B_n is a vector of length ratios defining the body geometry, α is the angle of attack, and β is the yaw angle. E_i is a vector of dimensionless numbers relating the specific formation enthalpies of the species to the specific kinetic energy of the free-stream gas (*e. g.*, $2E_2/U^2$), R_j is a vector relating the characteristic lengths associated with the chemical reactions to the characteristic length of the body, Le_i are the Lewis numbers giving the dimensionless species diffusion coefficients, and $c_{\infty i}$ is a vector giving the dimensionless concentrations of the species in the free stream. Even this long list of variables is not complete, as the vibrational characteristics of the molecular species have been omitted.

Up to and including β in the above list, the variables are the same as in cold hypersonics, in which the remaining variables that describe the thermodynamic and chemical properties of the gas can be replaced completely by a single variable, the ratio of specific heats, which, for a perfect gas, is a constant. Clearly, the more complex thermodynamics and chemistry of the hypervelocity flow requires many more parameters to be duplicated in the scale experiments than perfect-gas cold hypersonics. For example, in air at a free-stream speed of 5 km/s, it is necessary to include at least 5 species and 8 reactions, so that, if all the geometrical parameters are exactly duplicated, there remain over 20 dimensionless variables to match. In fact, as has already been indicated in the introduction, it is not possible to simulate both binary and three-body reactions simultaneously (except at full scale) because of the difference in their dependence on the density.

In special cases, however, the problem may be considerably simplified. For example, if the gas is especially simple, such as in a single (dissociating) diatomic gas, there is only a single E and there are only two R's. Only one of the R's can be matched, and, *e. g.*, in blunt body flows, it is best to match the binary dissociation reaction. With correct E, this automatically also causes Re, Le and Pr to be matched. Thus, the problem is reduced to

$$Q = Q(M, T_w/T_0, E, R, c_\infty).$$

If the Mach number is sufficiently high, and the bow shock is not of interest in regions where it becomes very weak, the Mach-number-independence principle is effective, and the number of independent parameters is down to 4. This situation can be satisfactorily simulated.

Where such simplifications are not possible, it becomes necessary to divide the flow field up into particular regions and to simulate these separately. This is sometimes referred to as component testing. It is especially important in combustion, where both binary and three-body reactions are active. For this reason engine combustors are often tested by connecting the inlet of the combustor directly to the exit of the facility nozzle, thus enabling testing at or near full size. Another example is the testing of the situation on the front of a body by placing only the nose shape into the test section, so that binary scaling and Mach-number independence apply.

2.1.2 Blunt Body Flows

Since heat flux is the big enemy in high-enthalpy flows, and heat flux is inversely proportional to the square root of nose radius, bodies with large nose radius play a dominant role in the field. Blunt body flows may be characterized in terms of dimensionless parameters defined in terms of conditions immediately after a normal shock. For such flows Wen and Hornung (1995) showed that it is possible to define a single reaction rate parameter and a single energy parameter even for complex gas mixtures:

$$\begin{aligned} \Omega &= \frac{\rho_s d R \Gamma}{\rho_\infty u_\infty^3 C_{ps}} \left(\sum_{i=2}^{n} h_{c_i} \frac{dc_i}{dt} \right)_s \\ \Lambda &= 1 - \frac{u_e^2}{u_s^2}, \end{aligned}$$

where ρ, d, R and Γ are density, characteristic length, the universal gas constant and inverse molecular weight, c_i are the species mass fractions, t is time, h is specific enthalpy, u is flow velocity and C_p is specific heat at constant pressure. The subscripts s and ∞ denote conditions immediately behind the shock and in the free stream respectively. The subscript c_i denotes partial differentiation. The subscript e denotes conditions at equilibrium after a normal shock. All of the variables in these parameters are determined by the free-stream conditions, the properties of the gas mixture and the shock-jump relations.

The parameter Ω may be thought of as

$$\Omega = \frac{\text{Energy absorption rate by chemistry}}{\text{Input rate of freestream kinetic energy}}, \tag{1}$$

and the parameter Λ characterizes the energy that goes into chemistry and vibration in terms of the energy at the shock.

Since Mach number independence applies in high-enthalpy blunt body flow, proper simulation is achieved by duplication of the independent parameters in

$$Q = Q(\frac{T_w}{T_0}, \Omega, \Lambda, c_\infty).$$

Thus, in the case of blunt body flows, one parameter for each of reaction rate and energy may be defined even for a complex gas mixture. Again, duplicating these automatically duplicates the Reynolds, Prandtl and Lewis numbers. These parameters were shown to characterize the features of high-enthalpy flow over spheres very well by Wen and Hornung (1995).

2.2 Power

It is really quite amazing how much power is in a hypervelocity flow. For example, a wind tunnel with a cross-sectional area of 1 m^2, in which the flow speed is 7 km/s, and the density is 0.01 kg/m^3 requires a power of 2 GW. This is roughly a tenth of a percent of the power consumption of the USA. It also corresponds to an energy flux of 2 GW/m^2, or 46 times that at the surface of the sun. It is clear, that this kind of power can not be sustained for long times.

Fortunately, it only takes a very short time to set up a steady flow over a model at such high speeds. Opinions differ about the necessary test time. A reasonably conservative value is

$$\tau = 20 \frac{L}{U_\infty},$$

where L is the model length and U_∞ is the free-stream velocity. With this value, the test time requirement for the above facility comes out to approximately 3 ms, so that the *energy* requirement is only 10 MJ. This energy can be stored over a long time and released during a short test period.

The power requirement is thus one of the reasons why short-duration facilities are necessary for high-enthalpy flow simulation. Another reason arises in the case of facilities that use a steady expansion to accelerate the flow from rest. In such facilities, the thermodynamic condition in the reservoir from which the gas is expanded is such that the specific enthalpy, h_0, has to be 20 MJ/kg or so. In air, at a pressure of 100 MPa, this corresponds to a temperature of about 9500 K. Hence, it is necessary to limit the time for which the materials containing the flow are exposed to these conditions. With the best materials available today, 3 ms is about the limit at the conditions quoted.

2.3 Instrumentation

This topic is one that deserves at least as much space as this whole paper, and it will not be possible to deal with it here, except for the purpose of pointing to its importance. Clearly, a test in a hypervelocity simulation facility is quite expensive. It is therefore most desirable to make as extensive a set of measurements as possible, each time such a test is performed. Unfortunately, the different forms of non-intrusive testing that exist at present require different degrees of expertise, which are seldom available at the same place as the test, because of the degree of sophistication that they often require.

Among the presently used routine measurement techniques, the following are available at all high-enthalpy test facilities: Surface pressure and heat flux measurement, Schlieren and shadow photography, and interferometry. Techniques that are applied less widely to high-enthalpy flows, but are very important for them, are mass spectrometry, spectroscopy, laser-induced fluorescence, and Raman spectroscopy.

The latter group of methods are able to measure species concentrations and temperature, and therefore provide extremely important data for the analysis of results from high-enthalpy facilities. Examples of where such methods have been applied to high-enthalpy flows are in the T3 shock-tunnel laboratory at the Australian National University in Canberra, at the HEG facility in Göttingen, Germany, and at CUBRC in Buffalo, N.Y.

3 Hypervelocity Simulation Facilities

In this section the principles of operation of the most successful types of high-enthalpy facilities are presented. The thermodynamical and chemical processes which the gas undergoes in the generation of the hypervelocity flow are given prominence in this, because they define and explain the most serious disadvantages of the facility types.

3.1 Reflected-Shock Tunnel

3.1.1 Configuration and Operation

By far the most used and most productive high-enthalpy simulation facility is the reflected shock tunnel. Fig. 1 shows a schematic sketch and a wave diagram of the device. Initially, the driver region is filled with high-pressure gas and a diaphragm separates it from the shock tube that is filled with the test gas at lower pressure. The shock tube is separated from a nozzle, attached to its other end, by a weak diaphragm. The nozzle and test section, as well as the dump tank, are initially evacuated. The test section and dump tank are not shown in the figure.

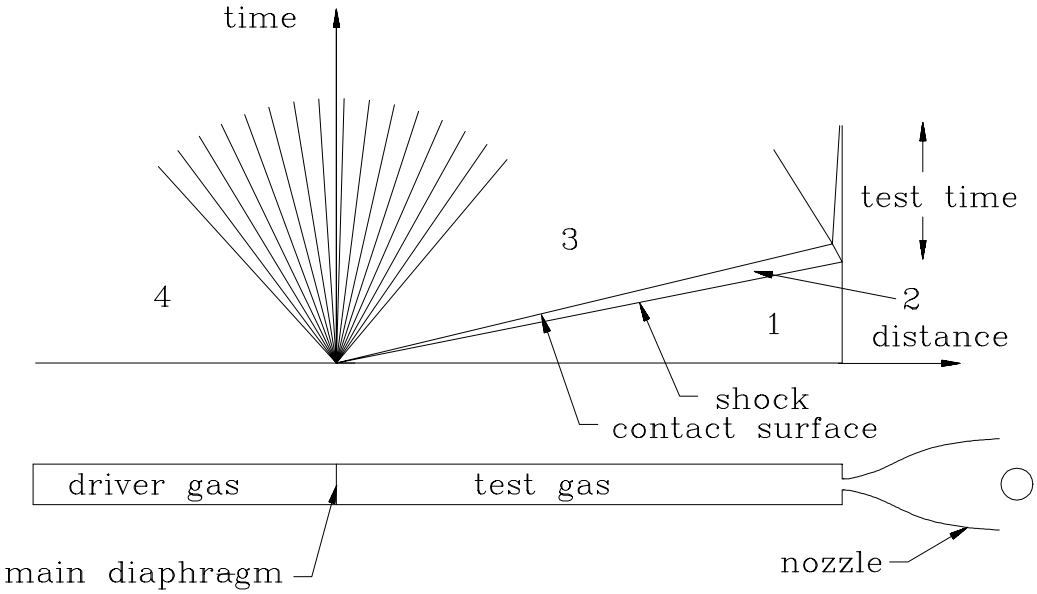

Figure 1: Schematic sketch of reflected shock tunnel and wave diagram. The separation between the shock wave and contact surface is exaggerated to show it better.

When the main diaphragm breaks, a shock wave propagates into the test gas, and an expansion wave propagates into the driver gas in such a way that the pressures and velocities in the region between the shock wave and expansion wave are continuous across the interface between the two gases. These processes are shown in the wave diagram of Fig. 1. The initial state of the driver gas, in region 4 of the wave diagram, is processed by the expansion wave to the condition in region 3, and the initial state of the test gas, region 1, is processed by the shock wave to the condition in region 2. The states 2 and 3 are determined by the expansion wave and by the shock wave and the requirement that

velocities and pressures must match across the boundary between 2 and 3. This may best be illustrated by a velocity-pressure diagram, shown in Fig. 2. The upper curve shows the locus of the states that can be reached from the initial condition of the driver gas via an expansion wave and the lower curve shows the states that can be reached from the initial state of the test gas via a shock wave. Their intersection represents the condition in regions 3 and 2, where pressures and velocities are matched. The solution thus corresponds to the intersection of the two curves in Fig. 2.

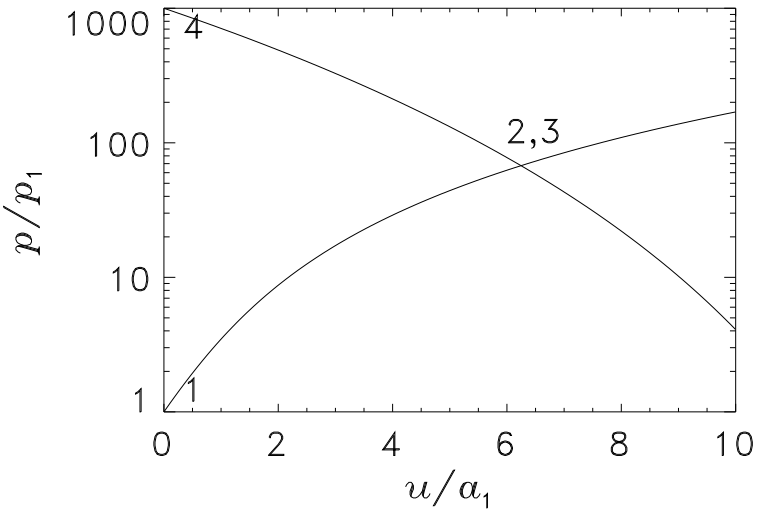

Figure 2: Example of velocity-pressure diagram for a shock tube. The pressure p is normalized with the initial pressure of the test gas, p_1, and the velocity u is normalized with the speed of sound in the test gas at condition 1, a_1. In this example the gases are treated as perfect gases with specific heat ratios γ_1 and γ_4 of 7/5 and 5/3 respectively. Also, the ratio of the speeds of sound a_4/a_1, the third parameter determining the solution, was chosen to be 5.

If a whole lot of such solutions are combined, the solutions can be shown parametrically in a diagram plotting the shock Mach number $M_s = U_s/a_1$ against the pressure ratio p_4/p_1. This is done in Fig. 3.

In the reflected shock tunnel, the state of the test gas in region 2 is processed further by the shock wave reflected from the closed end of the shock tube. This heats and compresses the gas even more than has already been accomplished by the primary shock, but it also brings the test gas to rest again. The primary shock breaks the thin diaphragm between the shock tube and the nozzle, thus allowing the test gas to expand in a steady expansion through the nozzle.

It is important to operate the shock tunnel in such a way that the interaction between the reflected shock and the contact surface does not produce any further waves. When conditions have been chosen in such a way that this is the case, this is referred to as tailored-interface operation. The condition behind the reflected shock is then the reservoir condition of the nozzle flow, and is referred to by the subscript 0.

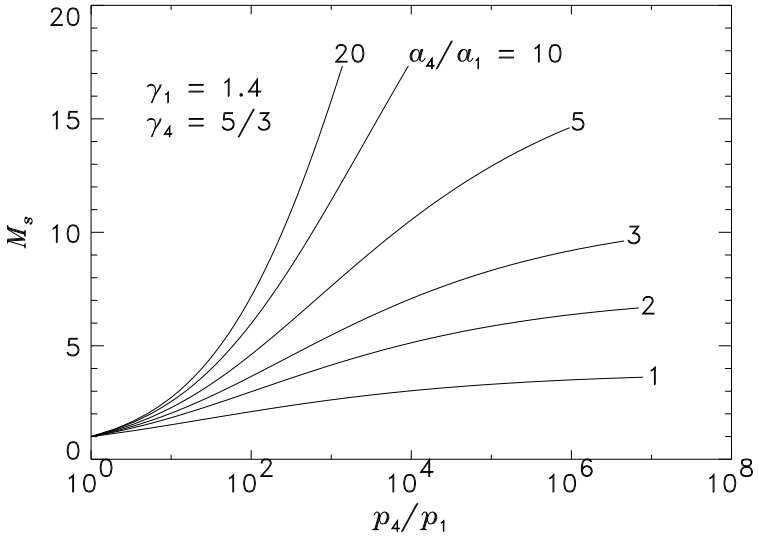

Figure 3: The shock tube equation for monatomic driver gas and diatomic test gas, both treated as perfect gases. Note the strong dependence of the shock Mach number on the speed of sound ratio. Real-gas effects modify this diagram only slightly.

The nozzle expansion converts the thermal energy of the stationary reservoir gas into ordered kinetic energy. In doing so, the maximum flow velocity achievable is

$$U_\infty = \sqrt{2h_0},$$

where h_0 is the specific enthalpy of the reservoir condition. Since it is necessary to achieve speeds around 6 km/s, the reservoir specific enthalpy needs to be in the vicinity of 18 MJ/kg. In a reflected shock tunnel, a very good approximation is

$$h_0 = U_s^2.$$

It follows that the shock speed has to be about 4.3 km/s, which, in air, corresponds to $M_s = 12.5$. Referring to Fig. 3, we see that this value may not be reached with pressure ratios less than 2000 unless a_4/a_1 exceeds 8. Since the test gas speed of sound is virtually fixed by the fact that we want to use air in a laboratory at room temperature, the driver-gas sound speed has to be high.

3.1.2 Driver-Gas Conditions

Various ways have been used to increase a_4. First, a light gas, either hydrogen or helium is used, and second, the driver gas is heated. Steady state heating is limited to about 800 K. This gives $a_4/a_1 = 4.8$ for helium driver gas and air test gas. Not only is this too low, but it is also expensive and dangerous to contain high-pressure and high-temperature gas for an extended period. A second method is to heat the driver gas relatively quickly by combustion of a limited amount of hydrogen and oxygen mixed with the driver gas

before the test. Mixtures in the proportions 14% hydrogen: 7% oxygen: 79% helium, give $a_4/a_1 \simeq 7$.

While this is just about enough, another, more convenient technique is to compress the driver gas adiabatically with a heavy piston. This method has the advantage that the driver gas is hot only for a very short time, and that (as in the combustion-heated driver) the high pressure required is produced automatically. However, it also means that the driver is short, with a moving end wall, so that waves traveling between the main diaphragm station and the piston cause disturbances to the shock. With adiabatic compression, values of a_4/a_1 up to 12 are easily achievable, and the value of this parameter may be adjusted by using mixtures of helium and argon as driver gas. Monatomic gases require smaller compression ratios for the same pressure and temperature gains.

An example of a free piston driven reflected shock tunnel is shown in Fig. 4. This is the facility known as T5 at GALCIT. Similar machines exist at Canberra (T3, recently de-commissioned) and Brisbane (T4) in Australia, see

`http://www.uq.edu.au/~e4dmee/t4.html`,

and larger ones at Göttingen in Germany (HEG), see *e. g.*, Hannemann (2002), and at Kakuda in Japan (HIEST), see *e. g.*, Itoh et al. (2002).

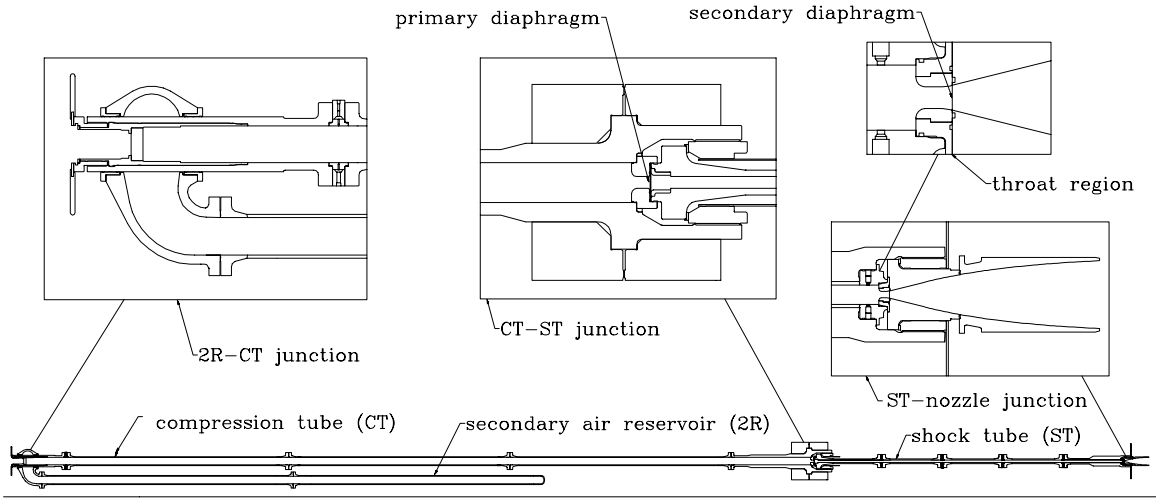

Figure 4: Sectional view of the free-piston reflected shock tunnel T5 at GALCIT, with blow-ups of some of the parts. On the left is the 30 m long compression tube, joined to the 12 m shock tube and nozzle on the right. The test section and dump tank are not shown.

The piston is accelerated in the compression tube (CT) by compressed air initially contained in the secondary air reservoir (2R), thus compressing the driver gas until the diaphragm burst pressure ($\simeq$ 90 MPa) is reached. The piston speed at rupture has to be sufficiently high ($\simeq$ 170 m/s) to maintain almost constant pressure after diaphragm rupture for a short time ($\simeq$2 ms). Thus, the free-piston driver is a constant-pressure driver, in contrast to the constant-volume driver of the conventional shock tunnel.

Another method of heating the driver gas is by a detonation wave traveling into a detonable mixture from the diaphragm end of the driver tube. This method has the

advantage that the diaphragm may be much thinner, since it only needs to withstand the relatively low pressure before detonation. It also produces a long driver which should produce a more uniform shock propagation than the free-piston driver. A disadvantage is that, with hydrogen, the combustion produces water. The NO invariably produced in the reflected shock tunnel is likely to combine with this to form a very hostile environment for instrumentation and models. A detonation-heated reflected shock tunnel is in operation at the Shock Wave Laboratory of the Technical University at Aachen, Germany.

3.1.3 Reservoir Conditions

The shock wave propagating along the shock tube generates a boundary layer on the shock tube wall which causes the shock to decelerate. This attenuation limits the length to diameter ratio of shock tubes to approximately 90. Since the test time is proportional to the shock tube length if there are no losses, the shock tube diameter effectively is one of the limiting factors on the test time.

As the shock speed needs to be approximately 4 km/s, the specific enthalpy after the primary shock is 8 MJ/kg. This corresponds to $h/R = 28{,}000$ K, where R is the specific gas constant for air at room temperature. The process undergone by the gas may be shown in a Mollier diagram, see Fig. 5. Here the initial state of the gas in the shock tube (state 1) is shown at $s/R = 24$ on the entropy axis as a square symbol, and the primary shock raises the state to the coordinates [30, 24000 K], (state 2) see dashed line. (Note: The lines joining points in this diagram are not the actual paths of the processes). Pressure and temperature are now 18 MPa and 4000 K. At this condition, part of the oxygen is already dissociated and some NO has been formed.

The reflected shock then increases h and s further, to the point [33.5, 60000 K], (state 0), where pressure and temperature are 100 MPa and 8000 K, see continuation of dashed line. The reflected shock also brings the gas to rest. The steady nozzle expansion then takes the gas down in enthalpy at constant entropy to the final point on the dashed line, which then represents the free stream conditions of the tunnel.

This is not quite correct, of course, because the nozzle flow does not usually proceed in thermodynamic equilibrium all the way down to this state. At some point in the nozzle flow, the density is no longer large enough to maintain the large number of three-body collisions between particles that is required for the atomic particles to continue recombining as the gas cools in the expansion. Such non-equilibrium states can not be represented in a Mollier diagram.

3.1.4 Nozzle-Flow Freezing

The recombination reactions stop fairly suddenly in the nozzle expansion and, because the composition of the gas remains constant after this point, the phenomenon is called nozzle-flow freezing. A well-known feature of freezing is that, for a given nozzle, the composition of the frozen gas depends only on the reservoir specific entropy s_0, and not on the reservoir specific enthalpy h_0 or reservoir pressure p_0. In the example of one of the nozzles of T5, the upper part of Fig. 6 shows the frozen composition plotted against s_0/R. As may be seen, the concentration of atomic oxygen in the flow increases as s_0/R increases, until at 34 the number densities of O_2 and O are equal. Also, the fairly high concentrations of NO are unavoidable.

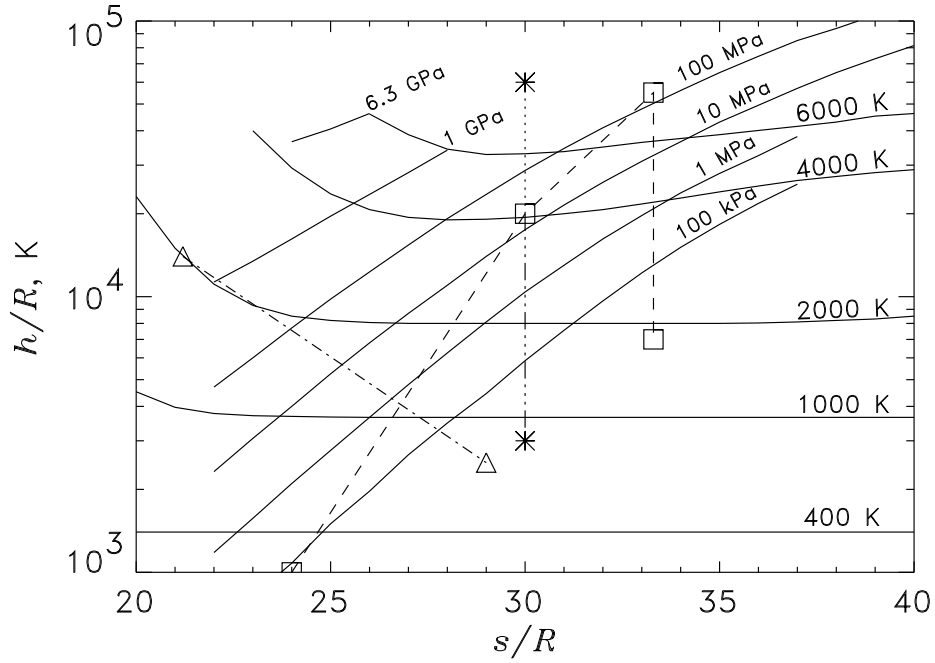

Figure 5: Mollier diagram for equilibrium air, showing lines of constant pressure and temperature. An example of the processes in a reflected shock tunnel is shown by the dashed line. The lower asterisk represents the exit condition in an expansion tube that starts with the same shock tube conditions as in the reflected shock example. The upper asterisk represents the effective reservoir state of the expansion tube. The triangles show reservoir and exit condition of the facility being developed at Princeton (MARIAH).. Note: The lines joining the symbols do not represent the actual paths of the processes between the states.

The lower part of Fig. 6 shows a Mollier chart of the reservoir state with the entropy axis aligned to that of the top figure. Here the enthalpy coordinate has been distorted to convert it into the velocity achievable from a given reservoir state. These two graphs show the relation between the composition of the free-stream gas and the reservoir pressure. For example, to achieve 6 km/s, a reservoir pressure of 100 MPa produces the composition corresponding to $s_0/R = 34.9$, while a reservoir pressure of 1 GPa at the same enthalpy would give the lower atomic oxygen concentration corresponding to $s_0/R = 31.6$. (Note: A pressure as high as 1 GPa would bring with it a great deal of additional problems). Fig. 6 also shows that the NO concentration remains constant as s_0 is decreased. This is unavoidable with high-enthalpy reflected shock tunnels.

3.2 Expansion Tube

3.2.1 Configuration and Operation

The expansion tube avoids some of the essential limitations of the reflected shock tunnel but introduces new ones. The expansion tube, like the reflected shock tunnel, first pro-

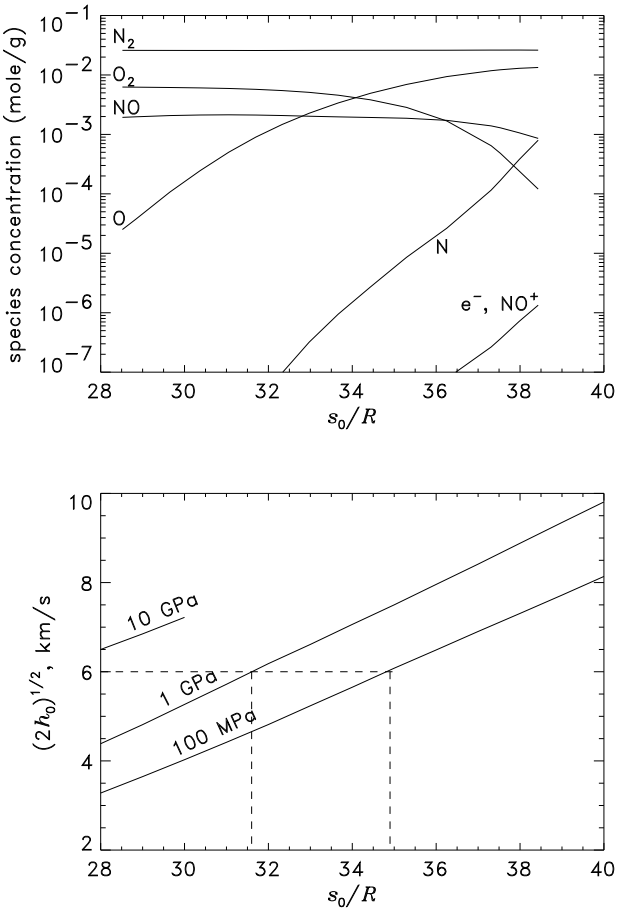

Figure 6: TOP: For a given nozzle, the exit composition depends only on the dimensionless reservoir entropy. Example of T5 nozzle. BOTTOM: Mollier chart of the reservoir state showing lines of constant reservoir pressure. The specific reservoir enthalpy axis is plotted in the form of the maximum achievable velocity. This shows how, at a given flow speed, the specific reservoir entropy, and therefore the exit composition, depend on the reservoir pressure.

cesses the test gas by propagating a shock wave through it, thus compressing, heating and accelerating it. The test gas is then not brought to rest as in a reflected shock tunnel, but accelerated further by an *unsteady* expansion. This is achieved by the arrangement shown schematically in Fig. 7 together with the wave diagram describing its operation.

In the expansion tube, a long acceleration tube usually of the same diameter as the shock tube is initially separated from the shock tube's downstream end by a thin secondary diaphragm. The pressures might have the initial values: 100 MPa, 100 kPa, 200 Pa in the driver, shock tube and acceleration tube respectively.

When the shock strikes the secondary diaphragm, it breaks, and the test gas acts as the driver for the shock propagating into the acceleration tube gas. The regions 10, 20 and 30 thus are analogous regions to those labeled 1, 2 and 3 in the shock tube. The processes undergone by the test gas are: 1-2 (shock), 2-3 (unsteady expansion). The conditions in

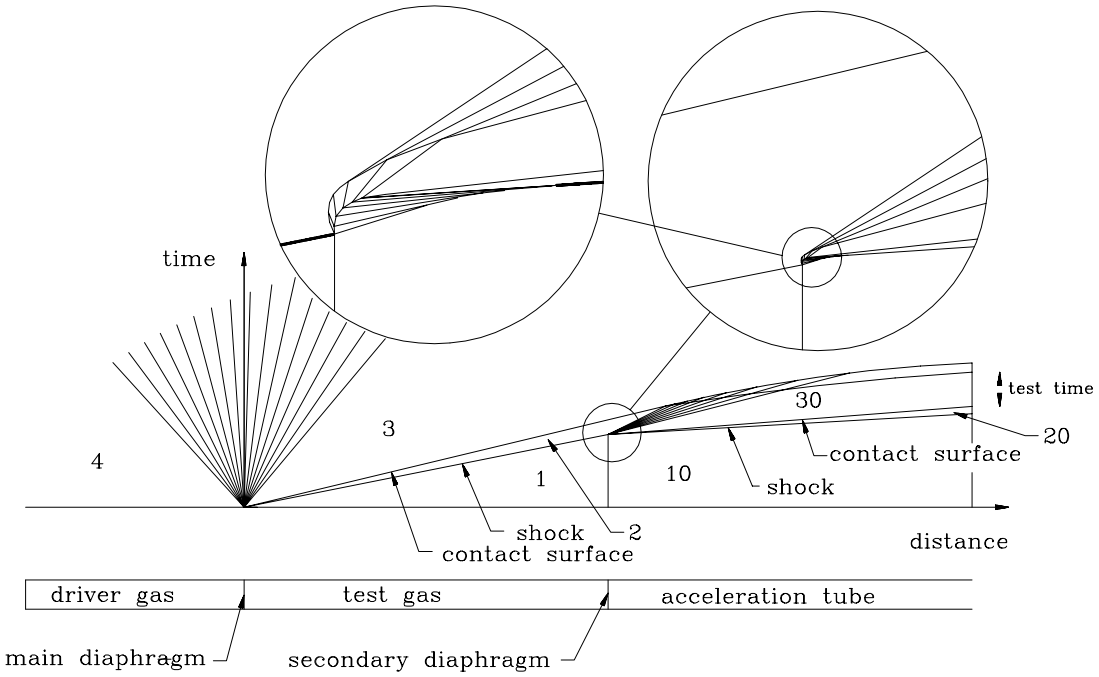

Figure 7: Schematic sketch and wave diagram of an expansion tube. The detail in the vicinity of the rupture of the secondary diaphragm is shown in two enlarged insets. The diaphragm is accelerated to the contact surface speed over a finite opening time. This causes a reflected shock that is accelerated by the left-running expansion wave transmitted from the diaphragm. Clearly, diaphragm opening time reduces the available test time.

the test gas after these processes may again be calculated by the shock tube equation. The result of such a calculation is shown graphically in Fig. 8. The test time is limited by the acceleration-gas test-gas contact surface, and by the leading edge of the reflection of the unsteady expansion from the driver-gas test-gas contact surface.

3.2.2 Effective Reservoir State

The expansion tube's thermodynamics may now be compared with that of the reflected shock tunnel in Fig. 5, where the lower asterisk marks the test condition of the expansion tube. The two first square symbols representing state 1 and state 2 are shared by the shock tunnel and expansion tube. The expansion tube takes the gas to a maximum temperature of 4000 K in this example, so that the atomic oxygen and NO concentrations may be kept much lower than in the shock tunnel.

At the same time, the effective specific reservoir enthalpy is more than twice the static enthalpy in region 2, since it is possible to gain total enthalpy in an unsteady expansion. To show the effective reservoir state of the expansion tube in Fig. 5 a second asterisk is plotted there, connected to state 2 with a dotted line to indicate that the gas never reaches this high enthalpy and pressure. The lower entropy of the expansion tube causes the effective reservoir pressure to be enormous. In our example, it is around 2 GPa. The static enthalpy h and static pressure p of the gas can remain low in the expansion tube, because the gas is not brought to rest after reaching state 2.

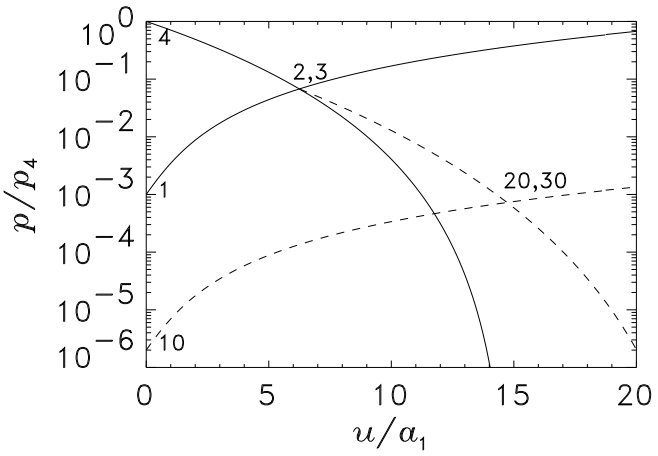

Figure 8: Velocity-pressure plot of the processes in an expansion tube. The full lines give the solution for region 2 and the dashed lines, representing the locus of conditions achievable via a shock wave from condition 10, and the conditions achievable via an unsteady expansion from condition 2, give the solution for the test condition, 20. In this example, the driver gas is monatomic and the test and acceleration gases are diatomic. All are considered perfect gases.

3.2.3 Free Stream Conditions

The test gas composition is practically that of state 2, because the density drops so quickly in the unsteady expansion that recombination of the atomic oxygen is not possible. Therefore it is best to operate the expansion tube with as low a value of T_2 as possible from this point of view.

If the expansion is taken to the same free-stream pressure as in the reflected shock tunnel, see Fig. 5, the free-stream temperature is seen to be much lower. This permits higher Mach number to be reached at the same h_0. Expansion tubes in operation include one at GASL in New York (HYPULSE) with a detonation driver, two free-piston driven expansion tubes in Brisbane, Australia (X-1 and X-3), and one at CUBRC in Buffalo, N.Y. (LENS-X).

3.3 Other Types of Facilities

A number of other types of facilities are in operation or are being considered. Among these the hypervelocity range is the most important. It employs a two-stage light gas gun to launch a model at the required speed into stationary gas in a long tube. This device is clearly much more expensive to operate than one in which the model is stationary. The model and instrumentation are also much more expensive, and it is difficult to test models that have high lift. However, the hypervelocity range is the only facility type in which good measurements of far wakes of bodies can be obtained.

There have been a number of other schemes, involving magneto-hydrodynamic accelerators or arc heaters. A relatively new idea being developed by a group at Princeton in

collaboration with Sandia National Laboratories, is the electron-beam-heated continuous flow facility (MARIAH), see, *e. g.*, Girgis et al. (2002). This scheme aims to keep the gas below 2000 K in order to prevent the formation of NO. In Fig. 5, the end points of the process are shown as triangular symbols joined by the chain-dotted line. The gas is expanded from a pressure of 1 GPa or more, and 2000 K. This makes use of the van der Waals effect that the isotherms curve up at low entropy, giving higher enthalpy without raising the temperature. In the example shown in Fig. 5, the gas has approximately 20% of the necessary total enthalpy in this condition. The remainder of the enthalpy is added in the supersonic region of the steady expansion by deposition of energy by means of magnetically controlled electron beams. Success depends critically on whether the enormous power levels required ($\simeq 1$ GW in the form of electron beams) can be produced and can be absorbed by the gas without causing non-equilibrium processes or damage to the nozzle walls. At this stage lower-pressure and lower-power energy deposition have been demonstrated. However, many problems remain to be solved before a useful facility can be produced based on this principle.

4 Limitations of the Main Facility Types

All the different facility types have limitations that constrain them to be operated in regimes where conditions are acceptable and where they work. To some extent, the regimes covered by different facilities complement each other. As in the previous sections the following discussion will concentrate on the two most important types, the reflected shock tunnel and the expansion tube.

4.1 Reflected Shock Tunnel

Part of the following discussion is concerned with the effects of increasing the size of a reflected shock tunnel. In these considerations it is assumed that the ratios of lengths remain constant. In particular, the length to diameter ratio of the shock tube, which is limited by friction and heat loss at the shock tube wall, is considered to have the same value. The best value for this ratio turns out to be close to 90.

There are four main limitations to the regime that can be covered by the reflected shock tunnel:

1. The departure of the composition of the free-stream gas from that of air.

2. The fact that the test gas is brought to rest before it is accelerated again produces very high temperatures at high pressures which causes a containment problem.

3. The test time is limited by the size, by driver-gas contamination and by the containment limitation.

4. The strength of the facility limits the pressure.

4.1.1 Free-Stream Freezing

It is clear from Fig. 6 that it is not possible to produce a free-stream gas composition that is free of NO, unless the reservoir temperature is kept below 2000 K. This is therefore a hard limitation of the device if one is interested in real-gas effects in air. To set an arbitrary limit, choose the case when the molecular oxygen concentration is half of that in air. Fig. 6 may now be used to translate this limit into a line in $h_0 - p_0$ space. The top part of the figure shows that this limit is reached at $s_0/R = 35.2$. The bottom part of the figure shows how p_0 and h_0 are related along this value of s_0. This relation is plotted in Fig. 9. As may be seen, an increase of p_0 moves the limit to significantly higher values of h_0.

This limitation may, strictly speaking, not be represented by a single curve in $h_0 - p_0$ space, because it is dependent on the size of the facility. However, since the recombination rate in the nozzle flow is proportional to the square of the pressure (other variables being the same) quadrupling the size of the facility would only lower the line by a factor of 2 in pressure.

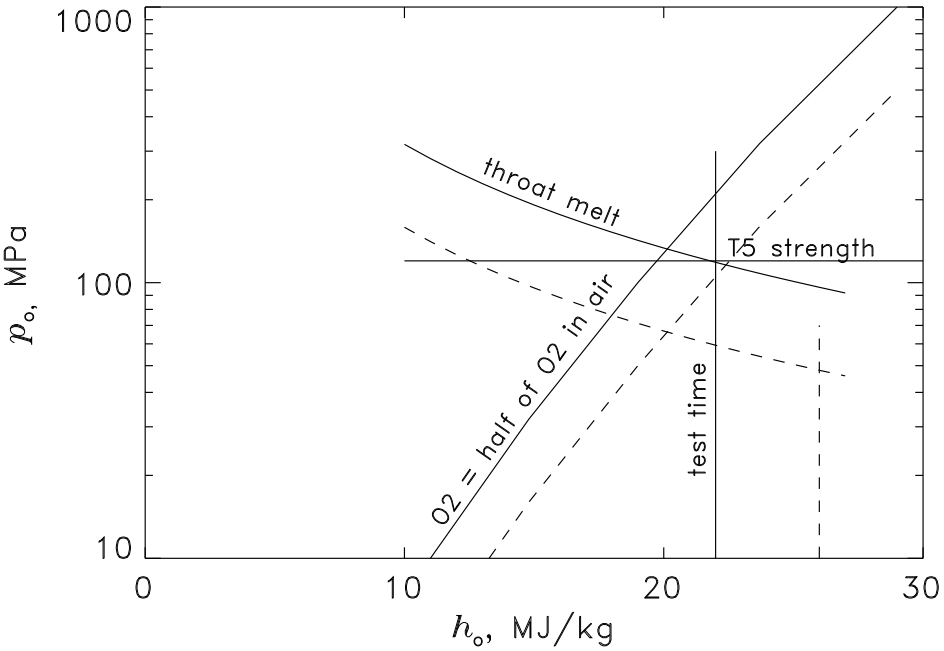

Figure 9: Limitations on the reservoir pressure and specific enthalpy of reflected shock tunnels. The full line represents a facility of the size of T5. The dashed lines are for a facility scaled up by a factor of 4.

4.1.2 Nozzle-Throat Melting

The high temperatures and pressures seen by the containing material in a reflected shock tunnel lead to the limitation that materials can not be found that will contain the conditions for the duration of the test without melting. From experiments in T5, a copper throat is found to melt at $p_0 = 100$ MPa, $h_0 = 20$ MJ/kg, when the exposure to high heat flux lasts approximately 3 ms. From this result, and from the properties of copper, the heat flux to the wall may be estimated using one-dimensional unsteady heat conduction theory to be $\simeq 2$ GW/m^2. This agrees roughly with semiempirical formulas for throat heating.

Starting from this experimental point, adjusting it for the difference in the properties of copper from those of the best material found so far (tungsten-copper alloy), and extending it according to approximate formulas, the curve shown in Fig. 9 results. The basis of the approximation of this extension is that the convective heat flux is proportional to the density and the cube of the velocity, and that the exposure time is inversely proportional to the velocity.

This curve also depends on the facility size. The surface temperature reached under a given transient heat load is proportional to the square root of the exposure time (other variables being the same). Since the heat flux is approximately proportional to pressure, quadrupling the size of the facility thus lowers the throat melt limit by a factor of 2 in p_0, which therefore kills half of the improvement of the upscale.

4.1.3 Driver-Gas Contamination

The time interval between the arrival of the shock and the arrival of the contact surface at the right-hand end of the shock tube (see Fig. 1) is the most important factor in determining the test time. The test time can not simply be calculated from one-dimensional computations, however, because the contact surface is in reality an extended region, and the complex interaction between the reflected shock and the boundary layer generated on the shock tube wall by the incident shock causes significantly earlier arrival of the driver gas at the nozzle throat. An example of this interaction is shown in the shadowgraph of Fig. 10 that illustrates how this interaction can cause early contamination.

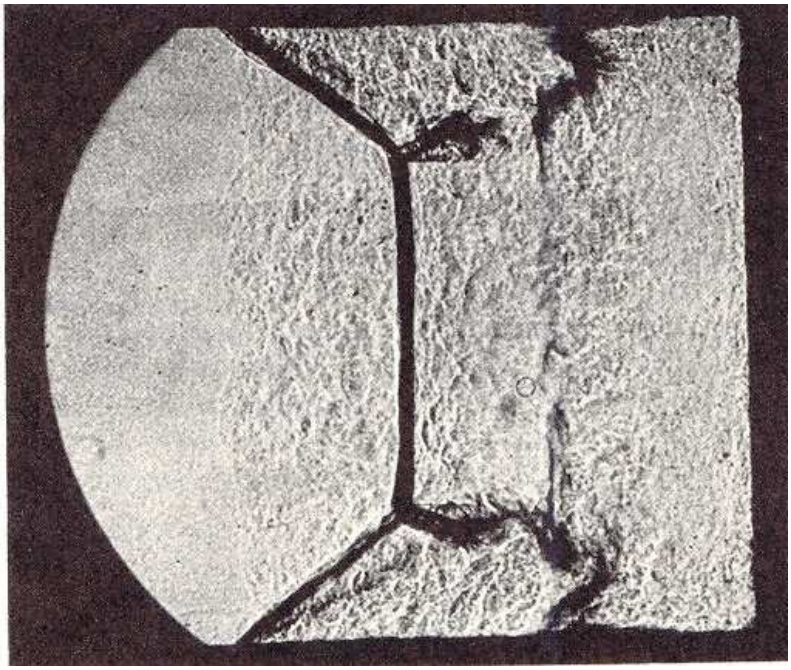

Figure 10: Shadowgraph of the interaction of the reflected shock with the shock tube wall boundary layer, illustrating mechanism of early contamination.

At a given h_0, the time interval between the arrival of the shock and the contact surface is directly proportional to the size of the facility (other variables being the same). As h_0 is increased, however, from the condition where the gas in region 2 is a perfect diatomic gas to where it is partially dissociated, this time interval changes down by almost a factor of 2. The speed with which the gas is drained from the reservoir through the throat into the nozzle increases as the square root of h_0. Fortunately, the test time requirement also decreases as the square root of h_0. However, the growth of the contact surface and the shock boundary layer interaction become more severe with increase of h_0. As h_0 is increased, there comes a point when the test time is no longer sufficient. Though only very sparse information is available on this limit, it may be placed roughly at 22 MJ/kg for the case of T5, and this is essentially independent of p_0.

Other things being equal, a scale increase increases the test time more than linearly, because the relative importance of the wall effects decreases. The test time *requirement* increases linearly with scale. The test time limit may therefore be expected to be moved

to slightly higher h_0 in a larger facility.

4.1.4 Strength, Scale Effects

Clearly, the strength of the facility merely limits the pressure at which it can be operated, and may be represented by a line at constant p_0.

To illustrate the effect of scaling up a facility from the size of T5 by a factor of 4, Fig. 9 also shows the displaced limits for the larger machine as dashed lines. This makes it clear that an increase of size makes strength relatively unimportant, since the throat-melt limit makes it impossible to operate at $p_0 > 70$ MPa, if $h_0 > 15$ MJ/kg in the facility scaled up by a factor of 4. As regards the throat-melt, test-time and strength limits, T5 appears to be close to the optimum scale. This was fortuitous, since the scale and strength were determined by other constraints.

4.1.5 Performance

In the region of $h_0 - p_0$ space within the above limitations, reflected shock tunnels can cover the space practically completely. In the case of the free-piston device, this can be achieved with tailored interface operation, because of the flexibility of the speed of sound ratio a_4/a_1 of this device.

4.1.6 Noise Measurement

4.2 Expansion Tube

As was pointed out in the description of the expansion tube, this facility type has the advantage that the material is exposed only to a fraction of the effective total pressure and only to a fraction of the total enthalpy. The stresses and heat loads are therefore not a serious limitation. Referring to Fig. 8 and Fig. 5 it becomes clear that for a given state 2, the effective values of p_0 and h_0 depend on the pressure p_{20} to which the flow is expanded in the unsteady expansion. It is therefore not meaningful to relate the extreme heating condition to the $h_0 - p_0$ space on this basis.

In the expansion tube a far more important concern is the short test time and the small test flow size. Consider for example a shock tube diameter of 100 mm. In the reflected shock tunnel, this provides a good flow for a nozzle exit diameter of typically 400 mm and a test duration of 1 ms at 18 MJ/kg. In the expansion tube, the same shock tube, driving an acceleration tube of the same diameter and 10 m length would produce a test flow of 100 mm exit diameter and 170 μs duration.

Fortunately, the size of the facility can be increased, since the penalty for size that plagues the reflected shock tunnel (melt limit) does not exist here. However, the test time limit remains, since the test time, which increases linearly with the size, only matches the increased test time *requirement*, which also increases linearly with size, unless the facility is deliberately made much larger than the models to be tested.

The friction losses in the acceleration tube set a limit on the length to diameter ratio. A reasonable maximum value is about 120. It turns out that a good shock tube length is then about 50 diameters. A rule of thumb for the optimum test time of an expansion tube is the time interval between the arrival of the primary shock and the arrival of the

shock tube contact surface at the end of the shock tube. This time is given approximately by

$$\tau \simeq 10\frac{d}{\sqrt{h_0}},$$

where d is the shock tube diameter. This is smaller than the test time requirement of $20L/V_\infty$, given in section 2.2, by a factor of 1.4 if the model size L is taken to be the tube diameter d. The model therefore has to be smaller than the largest model that could be tested in the facility if size were the only constraint.

Any attempts to expand the diameter of the expansion tube at the downstream end are therefore futile, since the model size is limited by the available test time, and not by the tube diameter. (This verdict may be relaxed if the flow studied is such that less test time than $20L/V_\infty$ is required.)

The most important problem in expansion tube operation is therefore the preservation of as much as possible of the test time. An obvious factor reducing the test time is the opening time of the secondary diaphragm, which is disregarded in the ideal expansion tube calculations above. In order to show the effect of finite diaphragm opening time, Fig. 7 shows as blown up insets two successive enlargements of a portion of the wave diagram. In the largest of these, the diaphragm is shown to accelerate from rest over a finite time to become the contact surface between the acceleration and test gas. The diaphragm thus causes the incident shock to be reflected. As the diaphragm accelerates, expansion waves are transmitted to the reflected shock, weakening it and eventually causing it to become the right edge of the unsteady expansion. On the acceleration tube side of the diaphragm, compression waves are transmitted to the right, which focus to form the acceleration tube shock. The time it takes to accelerate the diaphragm clearly reduces the test time .

The reduction in test time is roughly equal to the diaphragm opening time. This is given approximately by

$$t_D \simeq \sqrt{\frac{\rho\theta d}{p_2}},$$

where ρ is the density of the diaphragm material, θ is the diaphragm thickness and p_2 is the pressure in state 2. For a mylar diaphragm that is just strong enough to contain $p_1 = 100$ kPa, and a diameter of 300 mm, this gives an opening time of approximately 70 μs. On the basis of the above rule of thumb, the test time becomes 0.7 ms at 18 MJ/kg, so that the diaphragm opening time reduces the available test time by about 10%.

All of these considerations assume the flow to be one-dimensional, and serious consequences for the test time may be expected to result also from the wall effects on the structure of the two contact surfaces, and the three-dimensionality of the diaphragm rupture.

The composition of the test gas was assumed to be that of state 2 above. This is a little pessimistic, because some recombination will occur in the unsteady expansion during the later part of the test duration, where the gas has taken a longer time to traverse the expansion wave. This will therefore cause the composition to vary during the test time from an initial condition corresponding to that of state 2 to a final condition in which the atomic oxygen concentration, and to a lesser extent the NO concentration, are reduced slightly. The composition limit is almost independent of p_0. The molecular oxygen will be reduced to half the value in air at $h_0 \simeq 22$ MJ/kg.

Summarizing the limitations of the expansion tube, the emphasis has to be on the test time limit. Since the diaphragm opening time is independent of h_0, there comes a point where the enthalpy is limited by the test time. In the author's opinion, this limit is at 30 MJ/kg. The upper limit on p_0 is unimportant, since values in the GPa range are easily achievable.

The largest expansion tube in existence is LENS-X at CUBRC. The reader is referred to the website

`http://www.cubrc.org/WebModules/ServiceCategories/hypersonic.aspx`

5 Concluding Remarks

The thermodynamics, gasdynamics and scaling laws of hypervelocity flows, the power requirements, and the properties of containing materials, were shown to lead to the two main hypervelocity flow simulation facility types: The reflected shock tunnel and the expansion tube. The simplest forms of such devices were described, giving the logic that leads to them, and a comparison of their ranges of applicability. This was done with regard only to their main features, and many subtle points of their operation had to be omitted.

The hard limitations of the reflected shock tunnel constrain this device to be restricted to specific reservoir enthalpies below 22 MJ/kg and reservoir pressures below 90-200 MPa (depending on the enthalpy in the range 25-12 MJ/kg) at the size of the presently operating facility T5. Increase of size carries severe pressure penalties. The expansion tube's most severe restriction is the short test time. This is critically constrained by the behavior of the contact surface and the opening time of the secondary diaphragm. However, there appear to be no penalties for scale increase, and the reservoir pressure obtainable is extremely high. The upper limit for the specific reservoir enthalpy is approximately 30 MJ/kg on the basis of the free stream dissociation and test time constraints.

References

Girgis, I. G., Brown, G. L., Miles, R. B., and Lipinski, R. J. (2002). Fluid mechanics of a Mach 7-12, electron-beam driven, missile-scale hypersonic wind tunnel: Modeling and predictions. *Phys. Fluids*, 11:4026–4039.

Hannemann, K. (2002). High-enthalpy flows in the HEG shock tunnel: Experiment and numerical rebuilding. *22nd AIAA Aerodynamic Measurement Technology and Ground Testing Conference, St. Louis*.

Itoh, K., Ueda, S., Tanno, H., Komuro, T., and Sato, K. (2002). Hypersonic aerothermodynamic and scramjet research using high enthalpy shock tunnel. *Shock Waves*, 12:93–98.

Lukasiewicz, J. (1973). *Experimental Methods of Hypersonics*. Marcel Decker Inc. New York.

Wen, C.-Y. and Hornung, H. G. (1995). Non-equilibrium dissociating flow over spheres. *J. Fluid Mech.*, 299:389–405.